Production of the $N^*(1238)$ Nucleon Isobar by Photons of Energy up to 6 BeV*

CAMBRIDGE BUBBLE CHAMBER GROUP†

Brown University, Providence, Rhode Island, Cambridge Electron Accelerator, Cambridge, Massachusetts, Harvard University, Cambridge, Massachusetts, Massachusetts Institute of Technology, Cambridge, Massachusetts, University of Padova, Padova, Italy, and The Weizmann Institute of Science, Rehovoth, Israel

(Received 9 June 1967)

The reaction $\gamma+p \rightarrow N^*(1238)+\pi^-$ has been studied in a hydrogen bubble chamber exposed to a 4.8–6.0-BeV bremsstrahlung beam. This channel dominates the two-pion photoproduction reaction below the 1.05-BeV ρ^0-meson threshold, and at higher energies accounts for a significant part of the $p\pi^+\pi^-$ events after subtraction of the $p\rho^0$ channel. Total and differential cross sections, and $N^*(1238)$-decay angular correlations are presented over the energy range 0.5–1.8 BeV. These data are analyzed using a resonance model in which the reaction proceeds through the photoexcitation of the higher nucleon isobars—$N^{**}(1420)$, $N^{**}(1512)$, $N^{**}(1688)$, and possibly $N^{**}(1924)$. The only free parameters are the resonance strengths, which are fixed by a best fit to the total-cross-section curve. These same strengths account for the $N^*(1238)$ production angular distribution, but there remain some discrepancies between the predicted and observed N^*-decay angular correlations in the lowest-energy regions covered by our fit. Thus, although the total cross sections and production angular distributions require an appreciable contribution from $N^{**}(1420)$ excitation, the decay angular correlations tend to minimize the contributions of this resonance. However, satisfactory agreement with all the data may be obtained with a downward shift of the $N^{**}(1512)$ ($J=\frac{3}{2}^-$) resonance mass by ~50 MeV. Comparison is also made between our data and the one-pion-exchange model with final-state interaction. Unless this model is drastically modified (as for example in the calculations of Stichel and Scholz), agreement with the observations is poor.

I. INTRODUCTION

THIS is another in the series of papers reporting on the final results of the first bubble-chamber study of meson and hyperon production by photons of energy greater than 0.4 BeV. This experiment, performed at the Cambridge Electron Accelerator (CEA), utilized a 12-in. hydrogen chamber exposed to bremsstrahlung beams of maximum energy varying between 4.8 and 6.0 BeV. Some preliminary observations have previously been reported.[1] The experimental conditions, methods of analysis, cross sections, and laboratory angular distributions of observed products have been discussed in Ref. 2. Our observations and final conclusions on the reaction

$$\gamma+p \rightarrow p+\rho^0 \tag{1}$$

are discussed in an earlier paper.[3]

This paper is devoted mainly to a discussion of the reaction

$$\gamma+p \rightarrow N^*(1238)+\pi. \tag{2}$$

For photon energies below the threshold for ρ^0-meson production in reaction (1) (1.05 BeV), reaction (2) dominates the three-prong reaction

$$\gamma+p \rightarrow p+\pi^++\pi^-. \tag{3}$$

In the energy interval 1.1–1.8 BeV, reaction (2) continues to play an important role, but its rapidly decreasing cross section is soon overwhelmed by reaction (1) so as to be essentially lost in the background for photon energies greater than ~1.8 BeV.

In examining the details of reaction (2), we are led to the conclusion that our observations can be almost completely understood in terms of an isobar excitation mechanism [Fig. 1(b)],

$$\gamma+p \rightarrow N^{**} \rightarrow N^*(1238)+\pi, \tag{4}$$

involving only known isobars. On the other hand, a conventional one-pion-exchange (OPE) mechanism [Fig. 1(a)], with or without absorption in the final state,[4] cannot account for the observations for photon energies less than ~1.8 BeV.

* This work was supported in part through funds provided by the U. S. Atomic Energy Commission and by the Instituto Nazionale di Fisica Nucleare, Italy.

† Group members (by institution) are H. R. Crouch, Jr., R. Hargraves, B. Kendall, R. E. Lanou, A. M. Shapiro, and M. Widgoff, Brown University; G. E. Fischer, Cambridge Electron Accelerator; C. Bordner, Jr., A. E. Brenner, M. E. Law, U. Maor, T. A. O'Halloran, Jr., F. D. Rudnick, K. Strauch, J. C. Street, and J. J. Szymanski, Harvard University; P. Bastien, B. T. Feld, V. K. Fischer, I. A. Pless, A. Rogers, L. Rosenson, T. L. Watts, and R. K. Yamamoto, Massachusetts Institute of Technology; G. Calvelli, F. Gasparini, L. Guerriero, J. Massimo, G. A. Salandin, L. Ventura, G. Voci, and F. Waldner, University of Padova; A. Brandstetter, Y. Eisenberg, A. Levy, and E. E. Ronat, The Weizmann Institute of Science.

[1] H. R. Crouch *et al.*, Phys. Rev. Letters **13**, 636 (1964); **13**, 640 (1964); also, in *Proceedings of the International Symposium on Electron and Photon Interactions at High Energies, Hamburg, 1965*, edited by G. Höhler *et al.* (Deutsche Physikalische Gesellschaft, Hamburg, 1965), Vol. II, p. 21; and, in *Proceedings of the Second Topical Conference on Resonant Particles, Athens, Ohio, 1965* (Ohio University, Athens, Ohio, 1965), p. 476.

[2] Cambridge Bubble Chamber Group, Phys. Rev. **155**, 1477 (1967).

[3] Cambridge Bubble Chamber Group, Phys. Rev. **146**, 994 (1966).

[4] S. D. Drell, Rev. Mod. Phys. **33**, 458 (1961); F. Salzman and G. Salzman, Phys. Rev. **120**, 599 (1960); Phys. Rev. Letters **5**, 377 (1960); K. Gottfried and J. D. Jackson, Nuovo Cimento **34**, 735 (1964).

The inadequacy of the conventional OPE approach has also been noted by the Aachen-Berlin-Bonn-Hamburg-Heidelberg-München (ABBHHM) bubble-chamber collaboration,[5] using data in good agreement with ours. However, they have been reasonably successful in fitting their data with a model developed by Stichel and Scholz,[6] in which OPE theory has been drastically modified to achieve gauge invariance by including additional diagrams, in particular, one corresponding to $N^*(1238)$ exchange. However, the Stichel-Scholz computations do not include the resonance diagram [Fig. 1(b)], which is the one on which we have concentrated in this paper.

Previous analysis[7] of observations on single-pion photoproduction below $E_\gamma \sim 1$ BeV has indicated the importance of the resonance mechanism

$$\gamma + p \rightarrow N^{**} \rightarrow \text{nucleon} + \pi . \qquad (4')$$

Since the nucleon plus two-pion decay of the higher isobars is known to be appreciable,[8] and since decay into $\Delta + \pi$ accounts for an appreciable portion of this decay mode, we expect reaction (4) also to be significant in the energy range in which (4′) is important.

Thus, the resonance approach used in this paper and the one used by the ABBHHM collaboration[5] are complementary. Both lead to reasonable agreement with most of the data—the resonance model having greater success in describing the total and differential cross sections for Δ production and the Stichel-Scholz model describing better the Δ-decay angular distributions (see Sec. II). Further improved experiments are needed to clarify the relative roles of these different mechanisms in the reaction under consideration.

II. Δ-ISOBAR PRODUCTION IN THE REACTION $\gamma + p \rightarrow p + \pi^+ + \pi^-$

Three-prong events of this type can be unambiguously identified and analyzed as 3C events (three kinematical constraints), yielding a sample without appreciable contamination from reactions involving neutral products or other charged particles. Above 1.1 BeV, ρ^0-meson production [see reaction (1)] assumes increasing importance until it completely dominates the three-prong sample for $E_\gamma \gtrsim 1.8$ BeV.[3] In the analysis contained in this paper, we shall concern ourselves mainly with events produced by photons below 1.8 BeV.

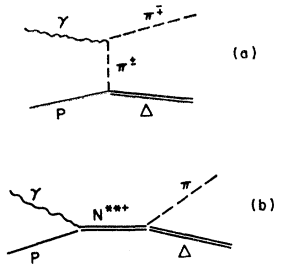

FIG. 1. Diagrams corresponding to possible mechanisms for the reaction $\gamma + p \rightarrow \Delta + \pi$. (a) One-pion exchange; (b) intermediate N^{**} resonance.

A. Mass and Charge Distributions

The observed $(p\pi^+)$ and $(p\pi^-)$ mass distributions are shown in Figs. 2 and 3. The curves shown are the result of the best over-all fits of the $(p\pi^+)$ and $(p\pi^-)$ invariant mass distributions assuming Δ production, three-body phase-space, and, above 1.1 BeV, ρ^0-meson reflections. We have assumed a relativistic Breit-Wigner form as described by Jackson[9] for the Δ mass distribution, with the resonant energy of 1238 MeV and a width $\Gamma(\Delta) = 120$ MeV. The $(p\pi^-)$ and $(\pi^+\pi^-)$ mass distributions, when appropriate account is taken of the Δ and ρ^0 resonances, show no evidence for any additional resonances (see Fig. 3).

Figure 2 demonstrates, through the dominating presence of the Δ^{++}, that reaction (2) is the main channel contributing to the two-pion production [reaction (3)] for photon energies below (and in the region of) the ρ^0-meson production threshold.

The final state (3) can result either from channel (2) with

$$\gamma + p \rightarrow \Delta^{++} + \pi^- \qquad (2')$$
$$\searrow$$
$$p + \pi^+ ,$$

or, alternatively, from

$$\gamma + p \rightarrow \Delta^0 + \pi^+ \qquad (2'')$$
$$\searrow$$
$$p + \pi^- ,$$

with relative amounts of Δ^{++} and Δ^0 depending on the reaction mechanisms. Thus, for example, the OPE mechanism [Fig. 1(a)] predicts

$$\Delta^0 : \Delta^{++} = 1 : 3 \qquad (5a)$$

as a result of isospin conservation at the $\Delta p\pi$ vertex; since the $p\pi^-$ decay mode of the Δ^0 has a branching ratio of $\frac{1}{3}$, the expected ratio as observed in reaction (2) is

$$\Delta^0(p\pi^-) : \Delta^{++}(p\pi^+) = 1 : 9 . \qquad (5b)$$

Exactly this same 1:9 ratio is predicted for a resonance absorption process [Fig. 1(b)] *provided the intermediate N^{**} has isotopic spin $T = \frac{1}{2}$*. For an intermediate N^{**} with $T = \frac{3}{2}$, on the other hand, the expected ratio is

$$\Delta^0(p\pi^-) : \Delta^{++}(p\pi^+) = 4 : 9 . \qquad (5c)$$

[5] Aachen-Berlin-Bonn-Hamburg-Heidelberg-München collaboration, in *Proceedings of the International Symposium on Electron and Photon Interactions at High Energies, Hamburg, 1965*, edited by G. Höhler *et al.* (Deutsche Physikalische Gesellschaft, Hamburg, 1965), Vol. II, p. 36; Nuovo Cimento **41**, 270 (1966); Phys. Letters **23**, 707 (1966).

[6] P. Stichel and M. Scholz, Nuovo Cimento **34**, 1388 (1964). Absorption corrections for this model were calculated by M. P. Locher and W. Sandhas, Z. Physik **195**, 461 (1966).

[7] Ph. Salin, Nuovo Cimento **28**, 1294 (1963).

[8] A. H. Rosenfeld *et al.*, Rev. Mod. Phys. **39**, 1 (1967); University of California Radiation Laboratory Report No. UCRL-8030 Rev., 1967 (unpublished). We adopt their notation, and henceforth refer to the $N^*(1238)$ as the Δ isobar.

[9] J. D. Jackson, Nuovo Cimento **34**, 1644 (1964).

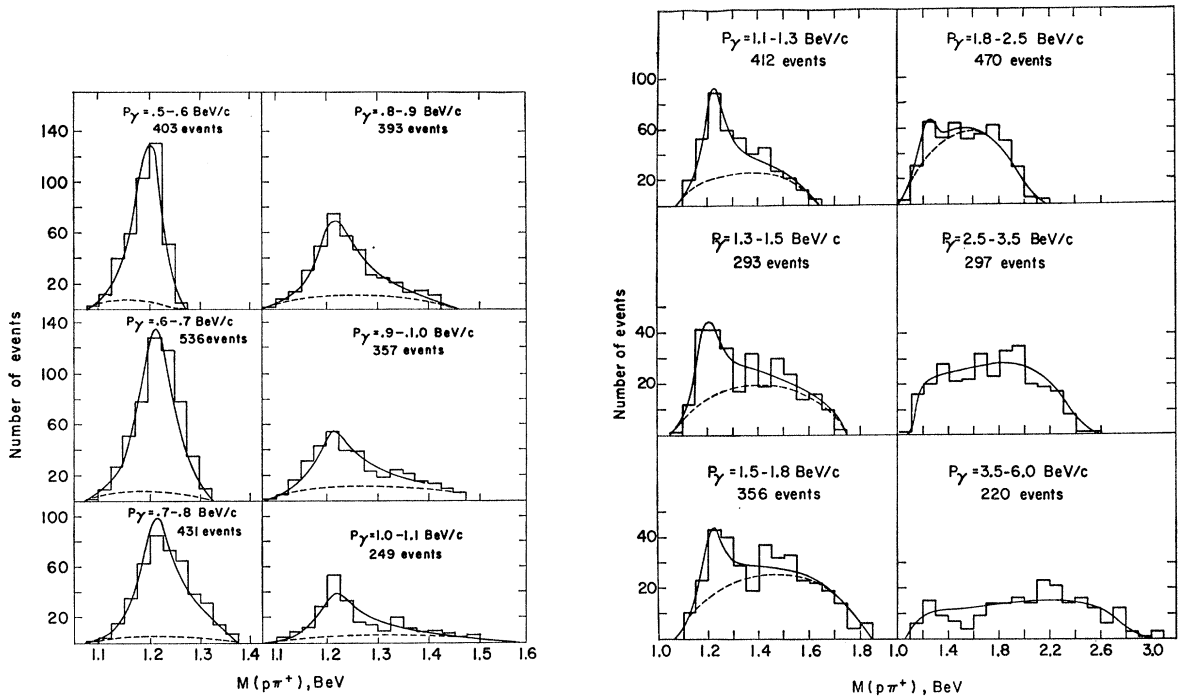

FIG. 2. Invariant mass distribution of the $(p\pi^+)$ in the reaction $\gamma+p \rightarrow p+\pi^++\pi^-$. The smooth curves are the best fits assuming a mixture of $(\Delta^{++}\pi^-)$, $(\Delta^0\pi^+)$, and $(p\pi^+\pi^-)$ phase space. Above 1.1 BeV, ρ^0 reflections are also added. The percentages are those listed in Table I. The broken curves represent the background contribution to the $p\pi^+$ mass plots (phase space, ρ^0 and Δ^0 reflections).

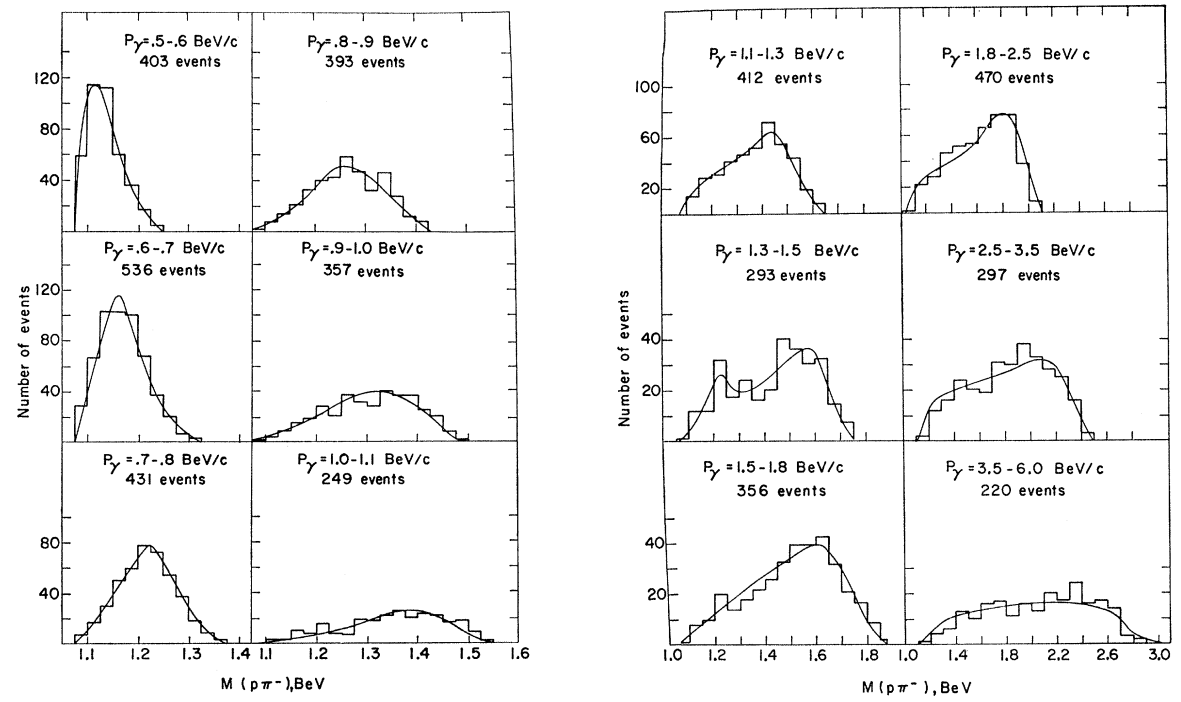

FIG. 3. Invariant mass distributions of the $(p\pi^-)$ in the reaction $\gamma+p \rightarrow p+\pi^++\pi^-$. The curves are the best fits assuming a mixture of $(\Delta^{++}\pi^-)$, $(\Delta^0\pi^+)$, and $(p\pi^+\pi^-)$ phase space. Above 1.1 BeV, ρ^0 reflections are added also. The percentages are listed in Table I.

TABLE I. Results of the best fits to the invariant mass distributions for obtaining the fraction of Δ^{++}, Δ^0, ρ^0, and phase space.

E_γ interval (BeV)	$\Delta^{++}\to p+\pi^+$ (%)	$\Delta^0\to p+\pi^-$ (%)	$\rho^0\to\pi^++\pi^-$ (%)	Phase space (%)	p_χ^2 (%)
0.4–0.5	84±10	0±15	···	16± 7	49
0.5–0.6	87± 5	0± 8	···	13± 3	43
0.6–0.7	88± 5	0± 5	···	12± 4	9
0.7–0.8	89± 4	0± 8	···	11± 3	94
0.8–0.9	66± 6	6± 6	···	28± 6	54
0.9–1.0	61± 6	9± 5	···	30± 7	26
1.0–1.1	71± 8	3± 6	···	26±11	16
1.1–1.3	45± 5	5± 4	32± 6	18± 6	71
1.3–1.5	32± 8	9± 7	35±10	24±10	3
1.5–1.8	23± 5	0± 4	48± 7	29± 6	25
1.8–2.5	11± 3	0± 3	62± 8	27± 8	0.5
2.5–3.5	4± 3	0± 3	72± 8	24± 8	29
3.5–6.0	4± 4	0± 4	81± 7	15± 6	24

Table I lists the best fits of the invariant mass distributions of the $p\pi^+$ and $p\pi^-$, to a sum of Δ^{++}, Δ^0, and ρ^0 (and their reflections), and to phase space. We list the obtained percentages of Δ^{++}, Δ^0, ρ^0 reflection, and phase space. The percent ρ^0 given in the table was obtained from the fits to the $\pi^+\pi^-$ distribution and is consistent with the best percent ρ^0 reflection required in the above $p\pi$ fits. The $\pi^+\pi^-$ mass distribution also was fitted to a Jackson-shape ρ^0 resonance.[9] We note that in Ref. 3 the ρ^0 percentages were obtained on the basis of a fixed-width Breit-Wigner resonance shape. The Jackson-shape ρ^0 gives consistently slightly lower ρ^0 percentages. The fraction of Δ^{++} given in Table I is insensitive to the assumed ρ^0 shape. We note that below 1.1 BeV, the best fits prefer essentially no Δ^0 production, although a ratio $\frac{1}{9}$ is nearly as likely.

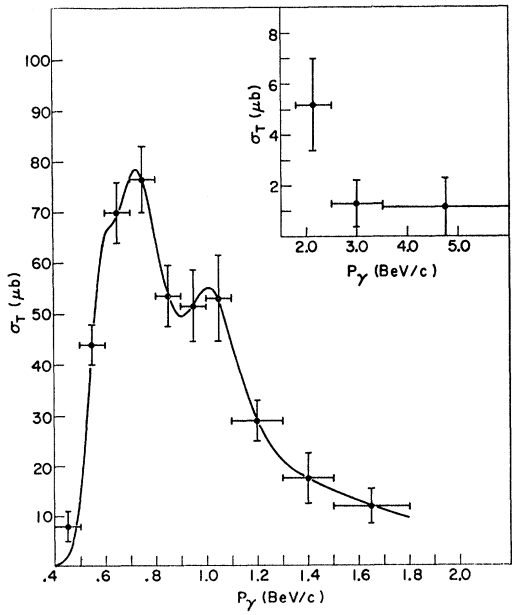

FIG. 4. Total cross section for the reaction $\gamma+p\to\Delta^{++}+\pi^-$, as a function of the γ-ray energy. The curve represents the best fit, row (4b) of Table III.

These results in themselves exclude the possibility of dominance of an intermediate $T=\frac{3}{2}$ state below ~1 BeV, but they do not permit a choice between OPE and a resonant mechanism dominated by $T=\frac{1}{2}$ intermediate states.

B. Total Cross Section for Δ-Isobar Production

The percentage Δ^{++} listed in Table I, together with the measured photon spectrum,[2] have been used to obtain the total cross section for Δ^{++} isobar production in reaction (3). These are shown in Fig. 4. The errors quoted represent a combination of statistical errors and fit errors involved in fitting the invariant mass distribution. The total Δ production can be directly obtained[10] from the Δ^{++} production.

We note the following outstanding features of this cross section: (1) the rapid rise from threshold to a peak at $E_\gamma\simeq 0.75$ BeV; (2) the rapid fall-off beyond the peak, with a possible shoulder in the cross section in the energy range, $E_\gamma\simeq 0.9$–1.1 BeV; (3) the relatively slow decrease in the region 1.3–1.8 BeV. We shall, in the following, attempt to explain all of these features in terms of photoexcitation of the four best known nucleon isobars of mass greater than the Δ, and their subsequent decay through the $\Delta+\pi$ mode [Fig. 1(b)].

The properties of these isobars[8] are summarized in Table II. Column 1 gives the number which we shall henceforth associate with the resonance. Columns 3 and 4 give the resonance parameters as deduced from pion-scattering data; the figures in parentheses in column 4 are the values we have adopted for the "effective" widths, larger in some cases than the accepted values, in order to take into account the energy resolution of our measurements.[11] Column 5 gives

[10] Note that as far as the elastic decays of the isobars are concerned, the peak cross sections eventually obtained [Eq. (12b)] for the reaction

$$\gamma+p\to N^{**+}\to N+\pi$$

include both decays $N^{**+}\to p+\pi^0$ and $N^{**+}\to n+\pi^+$. On the other hand, Fig. 4 and the resonance cross sections we shall deduce from it (Table III) refer only to the reaction

$$\gamma+p\to N^{**+}\to\Delta^{++}+\pi^-.$$

In order to calculate the branching ratio R for the two modes of N^{**} decay [Eq. (11)], one has to introduce a correction factor

$$G=\frac{\gamma+p\to N^{**+}\to(\Delta^{++}+\pi^-,\ \Delta^+\pi^0,\ \Delta^0+\pi^+)}{\gamma+p\to N^{**+}\to\Delta^{++}+\pi}.$$

Using the appropriate Clebsch–Gordan coefficients, one finds that

$$G_{1/2}=2,\quad\text{for isobar with } T=\tfrac{1}{2};$$
$$G_{3/2}=\tfrac{5}{2},\quad\text{for isobar with } T=\tfrac{3}{2}.$$

Obviously $G_{1/2}$ multiplies the cross sections σ_{01}, σ_{02}, and σ_{03} of Eq. (12a) while $G_{3/2}$ multiplies σ_{04}.

[11] A rough estimate of the sensitivity of the photon energy to the errors in the measured momenta for our 3C fits indicates that these increases of the widths quoted in Ref. 8, which are themselves at best of limited accuracy, are consistent with the resolutions of our measurements. Besides, we have ascertained that the fits to our data obtained using the smaller widths, while they emphasize somewhat more strongly than experimentally indicated the maxima and minima in the cross section, are not qualitatively different or substantially worse than those obtained using the broader widths adopted (in parentheses) in Table II, column 4.

TABLE II. Properties of nucleon isobars which can decay into $\Delta+\pi$, and their photoproduction and decay quantum numbers.

No.	$E_{\gamma,\mathrm{res}}^{(\mathrm{lab})}$ (BeV)	$M(N^{**})$ (MeV)	$\Gamma(N^{**})$ (MeV)	$\Gamma(N\pi\pi)/\Gamma(N\pi)$	T	J^P	Incident γ-ray multipole	Product pion l value
1	0.606	1420	~150(150)	~0.5(10)	$\frac{1}{2}$	$\frac{1}{2}^+$	$M1$	1
2	0.749	1512	120(150)	~0.5(1.0)	$\frac{1}{2}$	$\frac{3}{2}^-$	$E1(M2)$	0(2)
3	1.050	1688	100(150)	~0.5(1.0)	$\frac{1}{2}$	$\frac{5}{2}^+$	$E2(M3)$	1(3)
4	1.505	1924	~200(200)	~1.0(1.0)	$\frac{3}{2}$	$\frac{7}{2}^+$	$M3(E4)$	3(5)

the nucleon–two-pion to nucleon–single-pion branching ratio in the isobar decay where known or deducible from the data in Ref. 8. Since not all the two-pion decays are through the $\Delta+\pi$ channel, these values should, in principle, represent upper limits to the ratio $R\equiv\Gamma(\Delta+\pi)/\Gamma(N+\pi)$. We may also deduce this ratio from the analysis of our data together with data on single-pion production, assuming the validity of the resonance model. It turns out that the values of R so deduced are rather larger than those listed in column 5, and we have accordingly used (see below) the values of R given in parentheses in Table II, column 5. These values of R are required only for determining the *shape* of the heavier resonances [see Eqs. (9a) and (9b) below]. Fortunately, however, in the fitting of our $\Delta+\pi$ events, it turns out that the shapes are extremely insensitive to variations of R over a relatively large range. (One should note that the actual determination of the branching ratios R in this experiment is achieved by comparison of the peak cross sections of $\gamma+p\rightarrow N^{**}\rightarrow\Delta+\pi$ and $\gamma+p\rightarrow N^{**}\rightarrow N+\pi$.) Columns 6 and 7 give, respectively, the isotopic spin and the spin and parity of the isobar in question. Column 8 gives the possible photon multipoles capable of exciting the resonances, while column 9 gives the possible orbital angular momenta of the pion produced in the decay of the intermediate resonance $N^{**}\rightarrow\Delta+\pi$. In our interpretation, we have in all cases assumed only the lower of the two possible multipoles and pion l values.

In attempting to fit the cross-section curve, we have adopted for the energy dependence of the cross section a sum of Breit-Wigner resonances,

$$\sigma=\sum_{i=1}^{4} y_i^2|A_i|^2. \tag{6}$$

The y_i are parameters[12] whose squares represent the relative strengths of the different resonances, while the A_i's have been defined so as to contain the entire energy dependence of the resonance amplitudes[13]:

$$A_i(M)=\frac{\Gamma_{\Delta i}^{1/2}(M)}{(M_i-M)-i\Gamma_i(M)/2}, \tag{7a}$$

where M_i is the resonance mass, $M(E_\gamma)$ the total c.m. energy of the $\gamma+p$ system, and $\Gamma_i(M)$ the total width of the resonance,

$$\Gamma_i(M)\equiv\Gamma_{\Delta i}(M)+\Gamma_{Ni}(M). \tag{7b}$$

We assume that the only significant contributions to the total widths are the two decay modes: nucleon$+\pi$ (Γ_N), and $\Delta+\pi$ (Γ_Δ). The energy dependence of the partial widths are given by

$$\Gamma_{\Delta i}(M)=\frac{\langle(q/q_0)V_{li}(q/q_0)\rangle}{\langle(q_{ri}/q_0)V_{li}(q_{ri}/q_0)\rangle}\Gamma_{\Delta i}^{0}, \tag{8a}$$

$$\Gamma_{Ni}(M)=\frac{(q'/q_0)V_{l'i}(q'/q_0)}{(q_{ri}'/q_0)V_{l'i}(q_{ri}'/q_0)}\Gamma_{Ni}^{0}, \tag{8b}$$

where

$$\Gamma_{\Delta i}^{0}=\Gamma_{\Delta i}(M=M_i)=[R/(1+R)]\Gamma_i^{0}, \tag{9a}$$

$$\Gamma_{Ni}=\Gamma_{Ni}(M=M_i)=[1/(1+R)]\Gamma_i^{0}, \tag{9b}$$

and where q is the c.m. momentum for decay $N^{**}(M)\rightarrow\Delta+\pi$, q_{ri} is the c.m. momentum for decay $N^{**}(M=M_i)\rightarrow\Delta+\pi$, and V_{li} is the angular-momentum barrier penetration factor[14] for $N^{**}(M)\rightarrow\Delta+\pi$. The quantities q', q_{ri}', and $V_{l'i}$ are defined in analogous manner for the elastic decay mode $N^{**}\rightarrow N+\pi$ (N represents a nucleon). Γ_i^0 is the total width of resonance i for energy at resonance ($M=M_i$), and $\Gamma_{\Delta i}^0$ and Γ_{Ni}^0 are the corresponding partial widths at the resonance for the decay modes $N^{**}\rightarrow\Delta+\pi$ and $N^{**}\rightarrow N+\pi$, respectively. The parameter q_0 depends on the interaction range, and we have studied the effects on our resonance fits of varying it between 0.22 and 0.14 BeV/c, corresponding to a range of 0.8–1.4 F. The results are not at all sensitive to the exact choice of q_0; for the fits presented in this paper, a value of $q_0=0.22$ BeV/c was used.

Note that near threshold, the Γ's have the required q^{2l+1} momentum dependence, while for large $q\gg q_0$ the dependence goes over to that of phase space, $\sim q$.

[12] These parameters represent the partial width of the higher isobars for the decay into $N+\gamma$.

[13] Strictly speaking, the numerator of Eq. (7) should also include an incoming channel partial width depending on the incident proton energy, and could have a different energy dependence in different resonances owing to the different multipoles involved in their excitation (Table II, column 8). However, since the dependence of the width on E_γ will tend to be cancelled by the λ_γ^2 (k_γ^{-2}) dependence of the resonance production, we have for simplicity assumed this cancellation to be complete (see also the Appendix).

[14] J. M. Blatt and V. F. Weisskopf, *Theoretical Nuclear Physics* (John Wiley & Sons, Inc., New York, 1952), p. 361. For the l values involved in our interpretation, $v_0(x)=1$; $v_1(x)=x^2/(1+x^2)$; $v_2(x)=x^4/(9+3x^2+x^4)$; $v_3(x)=x^6/(225+45x^2+6x^4+x^6)$.

TABLE III. Parameters of best fit to $\gamma+p \rightarrow N^{**+} \rightarrow \Delta^{++}+\pi^-$ via photoexcitation model.

Energy range E_γ (BeV)	Best-fit parameters y_1^2	y_2^2	y_3^2	y_4^2	Probability χ^2	P_{χ^2} (%)	Calculated peak cross sections σ_{01}^T (μb)	σ_{02}^T (μb)	σ_{03}^T (μb)	σ_{04}^T (μb)
(1a) 0.7–0.9	···	6.29	···	···	0.75	39	···	79.2	···	···
(1b) 0.6–0.9	···	6.96	···	···	12.8	0.2	···	87.6	···	···
(1c) 0.7–1.0	···	6.64	···	···	10.8	0.4	···	83.6	···	···
(1d) 0.6–1.0	···	7.20	···	···	20.5	0	···	90.7	···	···
(2a) 0.7–1.3	···	5.83	2.88	···	0.07	99	···	73.4	36.7	···
(2b) 0.5–1.3	···	7.09	2.32	···	96.6	0	···	89.3	29.5	···
(2c) 0.7–1.8	···	5.85	2.96	···	1.00	96	···	73.6	37.7	···
(2d) 0.5–1.8	···	7.10	2.39	···	97.3	0	···	89.4	30.5	···
(3a) 0.7–1.8	···	5.84	2.83	0.41	0.04	99	···	73.5	36.1	4.10
(3b) 0.5–1.8	···	7.10	2.28	0.38	96.5	0	···	89.4	29.0	3.73
(4a) 0.5–1.8	2.07±0.03	4.80±0.07	2.63±0.07	0.26±0.07	0.12	99	48.5±0.7	60.4±0.9	33.6±0.9	2.52±0.7
(4b) 0.4–1.8	2.08±0.19	4.79±0.41	2.63±0.40	0.26±0.38	4.72	58	48.4±4.5	60.3±5.2	33.6±5.1	2.52±3.7

In the case of the $\Delta+\pi$ decay, the momentum-dependent factors in the widths $\Gamma_{\Delta i}(M)$ have been modified to take into account the finite width of the Δ isobar, which can be produced with a variable mass m^*. This modification consists of weighting the various possible decay momenta corresponding to a given value of the total decay energy M but different values of m^*, according to the relativistic Breit-Wigner weight function[9]:

$$dP(m^*)=\frac{\Gamma_\Delta(m^*)dm^*}{[m^{*2}-(1238)^2]^2+(1238)^2\Gamma_\Delta(m^*)^2}, \quad (10)$$

$$\Gamma_\Delta(m^*)=\Gamma_\Delta{}^0[Q(m^*)/Q]^3,$$

where $\Gamma_\Delta{}^0$ is the width of the Δ at its center (120 MeV), $Q(m^*)$ is the momentum of decay proton in the Δ rest frame, and $Q_0=Q(m^*=1238$ MeV). Thus the average over m^* in Eq. (8a) becomes

$$\langle xV_l(x)\rangle\equiv\int_{M_p+\mu}^{M-\mu} xV_l[x(m^*,M)]dP(m^*),$$

where $x=q/q_0$ and μ is the pion mass.

We emphasize again that, once we have fixed the resonance parameters (Table II), the only variable parameters[12] available for fitting the cross sections are the relative resonance strengths y_i^2 in Eq. (6).

We now describe our procedure for fitting the total-cross-section curve (Fig. 4), giving the values of the parameters corresponding to the various best fits in Table III:

(1) It would be simplest to fit the sharp peak at ~0.75 BeV to a single resonance, corresponding to excitation of the $N^{**}(1512)$ isobar. The first four rows of Table III demonstrate that this resonance is far too narrow to account for the observations. A reasonable fit [(1a) in Table III] can be obtained over the photon energy range 0.7–0.9 BeV only. As soon as we attempt to include even one extra data point on either side [rows (1b) and (1c)] or on both sides [row (1d)], the fits become much worse.

(2) The obvious next move is to add the well-established 1688-MeV isobar resonance (No. 3). Our best fit for the case of these two resonances only is given in row (2a) of Table III for a considerably extended energy range ($E=0.7$–1.3 BeV). It is again evident that this range cannot be extended to the lower energies without spoiling the fit. The higher-energy data (0.7–1.8 BeV) are well described by these two resonances [see rows (2b)–(2d), Table III].

(3) The inclusion of the $N^{**}(1920)$ resonance slightly improves the fit in the energy range 0.7–1.8 BeV [row (3a) of Table III]. However, row (3b) of Table III shows that the above three resonances cannot account for the low-energy data.

(4) In order to explain the rapid rise in the cross section at threshold on the basis of our model, we have no choice but to introduce an isobar of mass less than 1520. The obvious candidate for this role is the 1420 $P_{1/2}$ isobar, proposed by Roper.[15] When this resonance is also included, an excellent fit is obtained over the entire

TABLE IV. Contribution of different N^{**}'s to the total cross section for best fit [Table III, row (4b)].

E_γ (BeV)	$N^{**}(1420)$ (μb)	$N^{**}(1512)$ (μb)	$N^{**}(1688)$ (μb)	$N^{**}(1920)$ (μb)
0.45	1.17	0.30	0.01	0.
0.55	38.67	6.08	0.09	0.
0.65	32.67	35.35	0.61	0.
0.75	14.29	60.28	2.34	0.
0.85	8.83	37.34	7.96	0.01
0.95	6.38	21.43	23.75	0.02
1.05	5.02	14.19	33.55	0.07
1.20	3.81	9.16	15.75	0.34
1.40	2.94	6.16	6.54	2.02
1.65	2.31	4.37	3.48	1.69

[15] L. D. Roper, Phys. Rev. Letters **12**, 340 (1964); G. Belletini, G. Cocconi, A. N. Diddens, E. Lillethum, J. P. Scanlon, and A. M. Wetherell, Phys. Letters **17**, 708 (1966); I. M. Blair *et al.*, *ibid.* **17**, 789 (1966).

energy range, as seen in Fig. 4 and rows (4a) and (4b) of Table III.

It should be noted that an S_{11} pion-nucleon resonance ($\frac{1}{2}^-$ isobar) at $M^*\simeq 1500$ MeV, recently indicated in some phase-shift analyses[16] and, particularly, invoked to account for the rapid rise of the η-meson production cross section near its threshold, would not be of any use in explaining the threshold behavior of the $\gamma+p\to\Delta+\pi$ reaction. Its decaying into $\Delta+\pi$ would require $l=2$, and the angular-momentum barrier would thus cause its cross section to rise even more slowly than either the 1420- or 1512-MeV resonance production. There could, of course, be some production through this channel hidden in the strong 1512 resonance, as there could also be some production in possible $\frac{5}{2}^-(T=\frac{1}{2})$ or $\frac{1}{2}^-(T=\frac{3}{2})$ resonant channels, recently postulated in this energy range. Although we have not felt that our data are sufficiently accurate or detailed to attempt a fit with more resonances or more variable parameters, we can certainly not exclude the presence of these other resonances as a result of this analysis. Furthermore, as we shall see, the comparison with the angular distributions indicates that our assumptions are not completely adequate to account for all of the observations.

The results of our fitting of the cross-section curve, summarized in Table III, together with the cross sections for single-pion production, as measured in previous experiments,[17] can also be used to obtain an estimate of the branching ratio in the decay of the higher isobars,

$$R_i=\frac{\Gamma(N_i^{**}\to\Delta+\pi)}{\Gamma(N_i^{**}\to\text{nucleon}+\pi)}. \tag{11}$$

Thus, using the values of the peak cross sections of Table III, taking into account the corrections for unobserved Δ decay modes,[10] and taking for our best fit row (4b) of Table III, we obtain for the peak cross sections of the reactions $\gamma+p\to N_i^{**+}\to\Delta+\pi$

$$\begin{aligned}
\sigma_{01}{}^T&=(48.8\pm4.5)\times2\ \mu\text{b},\\
\sigma_{02}{}^T&=(60.3\pm5.2)\times2\ \mu\text{b},\\
\sigma_{03}{}^T&=(33.6\pm5.1)\times2\ \mu\text{b},\\
\sigma_{04}{}^T&=(\ 2.5\pm3.7)\times\tfrac{5}{2}\ \mu\text{b}.
\end{aligned} \tag{12a}$$

These assume, of course, that all observed $\Delta\pi$ production arises from intermediate isobar excitation, an assumption which is not likely to be correct at the higher energies.

[16] L. D. Roper, R. M. Wright, and B. T. Feld, Phys. Rev. **138**, B190 (1965); P. Auvil, C. Loverlace, A. Donnachie, and A. T. Lea, Phys. Letters **12**, 76 (1964); B. H. Brandsen, P. J. O'Donnell, and R. G. Moorhouse, *ibid.* **11**, 339 (1964); P. Bareyre, C. Brickman, A. V. Stirling, and G. Villet, *ibid.* **18**, 342 (1965).

[17] R. M. Worlock, Phys. Rev. **117**, 537 (1960); K. Berkelman and J. A. Waggoner, *ibid.* **117**, 1364 (1960); R. L. Walker, in *Proceedings of the International Conference on Photon Interactions in the BeV Energy Range*, M.I.T., *1963* (MIT Press, Cambridge, Massachusetts, 1965), p. IV–1; H. De Staebler, Jr., E. F. Erickson, A. C. Hearn, and C. Schaerf, Phys. Rev. **140**, B336 (1965); S. D. Ecklund and R. L. Walker, Phys. Rev. **159**, 1125 (1967).

In order to compare with the single-pion production data, we have assumed the resonance model and treated the available data[17] on the reaction $\gamma+p\to N+\pi$ in precisely the same fashion as our own. Thus, we have used as the single-pion production amplitudes

$$A_i'=\frac{\Gamma_{Ni}{}^{1/2}(M)}{(M_i-M)-i\Gamma_i(M)/2}, \tag{7a'}$$

with the factors as previously defined [Eqs. (7)–(9)]. In the analysis of these data, no indication of appreciable effects of the $N^{**}(1420)$ resonance was observed, which leads to the conclusion that $R_1\gg1$, i.e., that the decay of this isobar is highly inelastic through the $\Delta+\pi$ mode. The peak cross sections that we get from our fitting procedure to the data on the reaction $\gamma+p\to N_i^{**+}\to N+\pi$ are[10]

$$\begin{aligned}
\sigma_{02}{}^T&\sim115\ \mu\text{b},\\
\sigma_{03}{}^T&\sim\ 41\ \mu\text{b},\\
\sigma_{04}{}^T&\sim\ \ 4\ \mu\text{b},
\end{aligned} \tag{12b}$$

from which, using Eq. (12a), we obtain

$$\begin{aligned}
R_2&\sim1,\\
R_3&\sim1.5.
\end{aligned}$$

These may be compared with the values from Ref. 8 listed in Table II. Note that because of the small contribution of the 1920 resonance, the value of $\sigma_{04}{}^T$ has very large uncertainties and is rather sensitive to the shape of the high-energy tail of the order resonances. Thus the value of R_4 in the present experiment cannot be reliably determined.

It is noteworthy that the interpretation of the reactions $\gamma+p\to N+\pi$ and $\gamma+p\to\Delta+\pi$, as resulting predominantly from the excitation of higher isobars, indicates inelasticities consistent with, if somewhat larger than, the generally accepted values for $N^{**}(1512)$ and $N^{**}(1688)$. The value of R obtained for the $N^{**}(1420)$ resonance is considerably greater than the estimates based on other data.[8,16]

We conclude that the cross-section curve for Δ isobar production in reaction (3) is entirely consistent with the assumption of excitation of the isobars listed in Table II. By adjusting the relative strengths of the individual isobar contributions, all the features of the cross-section curve can be fit. In obtaining this fit, at least the first three of the four isobars are needed.

C. Angular Distribution of Isobar Production

Figure 5 show the c.m. production angular distributions of the Δ^{++} isobar. The angle is with respect to the direction of the incident photon. The events plotted are those for which $1.15\ \text{BeV}\leq M(p\pi^+)\leq1.30\ \text{BeV}$ (Fig. 2). Owing to the dominance of Δ^{++} production below the ρ^0-meson threshold, we have not attempted to subtract any background for the low-energy data.

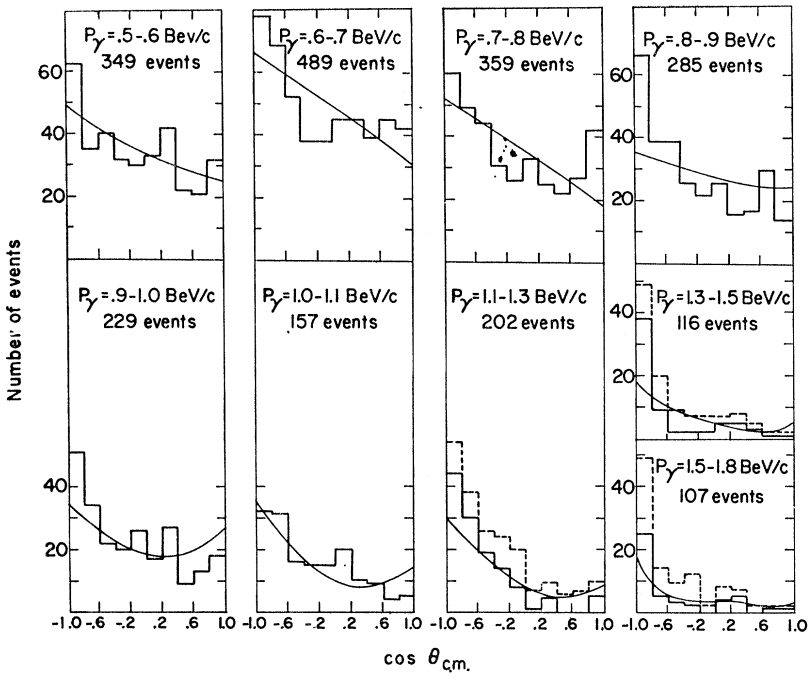

FIG. 5. Production angular distributions for the Δ^{++}, $[M(p\pi^+)=1.15$–1.30 BeV$]$ in the reaction $\gamma+p\rightarrow\Delta^{++}+\pi^-$. The curves are calculated on the basis of the y_i's given in row (4b) of Table III. For $P_\gamma>1.1$ BeV/c, the broken histograms represent the data before the background subtraction.

Above 1.1 BeV, however, a background subtraction has been performed with the background angular distribution assumed to correspond to the observed angular distribution in the $(p\pi^+)$ mass range $1.40\leq M(p\pi^+)\leq 1.55$ BeV.

Different assumptions about the mechanism for the $\gamma+p\rightarrow\Delta+\pi$ reaction lead to different predictions regarding the production angular distribution, as well as for the polarization and consequent decay angular correlations of the Δ.

Expressions for the predicted angular distribution are derived in the Appendix for the resonance model [Eq. (A3)]. The smooth curves shown in Fig. 5 correspond to the choices of the free parameters y_i based on the best fit to the total-cross-section curve as given in row (4b) of Table III.

In general, the predictions are in excellent accord with the experimental data. Specifically, we again note that the inclusion of the effects of the 1420-MeV isobar improves considerably the production-angular-distribution fits at the low energies.

It should be noted that the above fits do not include the possible contributions from a number of additional resonances in the 1.4–1.8-BeV region recently discussed in the literature.[8]

Our data do not exclude some contribution of Δ

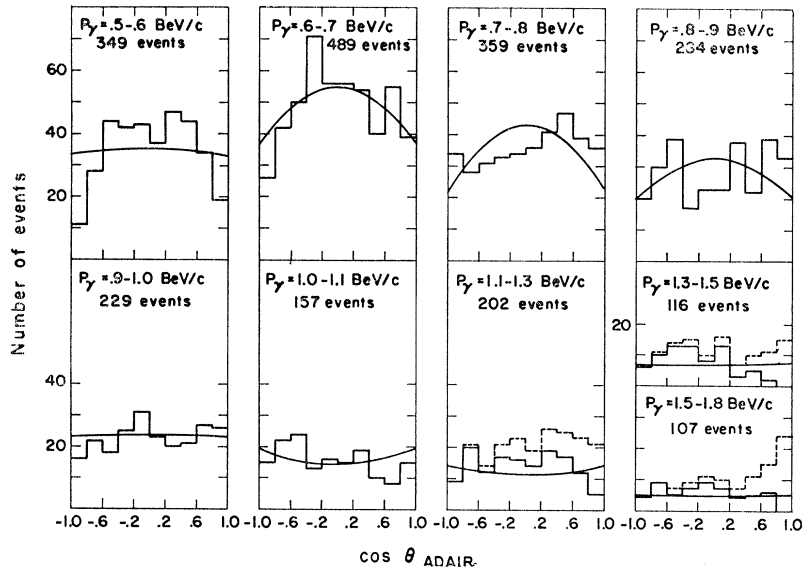

FIG. 6. Adair angular distributions for the decay correlation between the incident photon and decay pion π^+ in the reaction sequence $\gamma+p\rightarrow\Delta^{++}+\pi^-$, $\Delta^{++}\rightarrow p+\pi^+$. The curves are calculated on the basis of the y_i's given in row (4b) of Table III; for $P_\gamma>1.1$ BeV/c, the broken histograms represent the data before background subtraction.

production via the OPE mechanism [Fig. 1(a)]. This would cause a somewhat larger peaking in the backward direction for the Δ production angular distribution, which is not inconsistent with our data.

Taken as a whole, the observed Δ production angular distributions are in accord with the hypothesis of a dominant resonant production mechanism for the process $\gamma+p\rightarrow\Delta+\pi$, for photons of energy $\lesssim$1.8 BeV.

D. Decay Angular Correlations

The angular distributions of the decay pion in the Δ^{++} rest system with respect to the direction of the incident photon in the γ-p c.m. system (commonly referred to as the Adair angle α) are shown in Fig. 6. The spin-density matrix elements as a function of P_γ are shown in Fig. 7. The selection of events is identical with those used for the production angular distributions, and a similar background subtraction has been carried out for $E_\gamma>1.1$ BeV. The solid curves are the predictions of the resonance theory, using the same parameters of row (4b), Table III.

Angular-correlation theory, as described in the Appendix for the resonance model, leads to definite predictions for the polarization of the product Δ and, consequently, for the angular distribution of its decay in its own rest frame.

Although most of the qualitative features of the observed Adair-angle distributions are given by the theory, the fit in detail, using our "best" parameters from the cross-section fit, leaves much to be desired. Thus, in those regions dominated by the 1512-MeV isobar (which is the most important in our analysis) the theory predicts a $(5-3\cos^2\alpha)$ distribution [$\rho_{33}{}^A=\frac{3}{8}$; see Appendix, Eqs. (A4) and (A10)]. The effects of both the 1420- and the 1688-MeV isobars is to render the distribution more isotropic. However, our data indicate a distribution close to $(5-3\cos^2\alpha)$ only at the lowest energies (below the 1512 resonance), becoming rapidly more isotropic with increasing energy, and already rather flat in the region of the 1512-MeV resonance; it is as though the energy of the 1512 resonance was shifted downward by $\sim$50 MeV. Indeed, if one repeats the fits with the $\frac{3}{2}^-$ resonance at 1460 MeV (instead of 1512 MeV), one still obtains a good fit to the total cross sections for a new set of y_i's, with the contribution of the 1420 resonance much reduced. This new set of y_i's produces density matrix elements which are in considerably better agreement with our experiments. The best fit was with resonance No. 2 as $N_{3/2}{}^{-}{}^{**}(1460)$ yields values of $y_i{}^2$'s: $y_1{}^2=0.44$, $y_2{}^2=10.6$, $y_3{}^2=2.75$, $y_4{}^2=0.086$. [Compare with row (4b), Table III]. The resulting spin-density matrix elements are shown as broken lines in Fig. 7. These are in better agreement with the experimental data. Since angular distributions and decay correlations are particularly sensitive to even small admixtures of other (possibly resonant) states, which have been neglected in our analysis, we might be able to obtain further improvements by the inclusion of appropriate additional states.

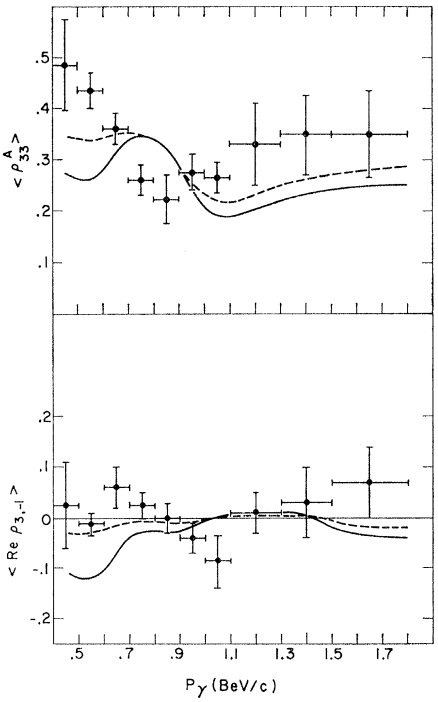

FIG. 7. Spin-density matrix elements for the Δ^{++} decay. $\langle\rho_{33}{}^A\rangle$ describes the Adair angular distribution; $\langle \mathrm{Re}\rho_{3,-1}\rangle$ describes the Treiman–Yang distribution. Solid curves are calculated on the basis of y_i's of row (4b) of Table III. The broken curve represents a fit based on the $\frac{3}{2}^-$ resonance shifted to 1.460 BeV (see text).

The Adair angle is not the most convenient one for a comparison with OPE theory; instead, it is usual to consider the angle between the incident and decay protons in the Δ isobar rest frame (OPE or Gottfried-Jackson[4] angle β). Simple OPE theory predicts a $(1+3\cos^2\beta)$ distribution, or $\rho_{33}{}^{GJ}=0$. Although the final-state interactions will tend to distort this strong correlation, they are, however, not expected to lead to any qualitative change in it.[18] Our observed spin-density matrix elements, describing the OPE distribution $\rho_{33}{}^{GJ}$ [see Eq. (A4)], are shown in Fig. 8 as function of the incident photon energy. The pure OPE prediction is $\rho_{33}{}^{GJ}=0$, in obvious contradiction with our observations. Absorption effects in the final state could raise $\rho_{33}{}^{GJ}$ to $\sim$0.10,[18] but this is also in clear disagreement with the data of Fig. 8 for the lower energies ($E_\gamma<1.8$ BeV).

It is interesting to note that the model of Stodolsky and Sukurai,[19] in which a "photonlike" ρ meson (i.e., with helicities ±1 only) is substituted for the exchanged pion in Fig. 1(a), gives rise to a $(5-3\cos^2\beta)$ angular correlation[20] over all energies. However, this model

[18] P. C. M. Yock, Ph.D. thesis, M.I.T., 1965 (unpublished).

[19] L. Stodolsky and J. J. Sukurai, Phys. Rev. Letters **11**, 90 (1963).

[20] This is simply the well-known angular distribution of the pions resulting from photoexcitation of the Δ resonance.

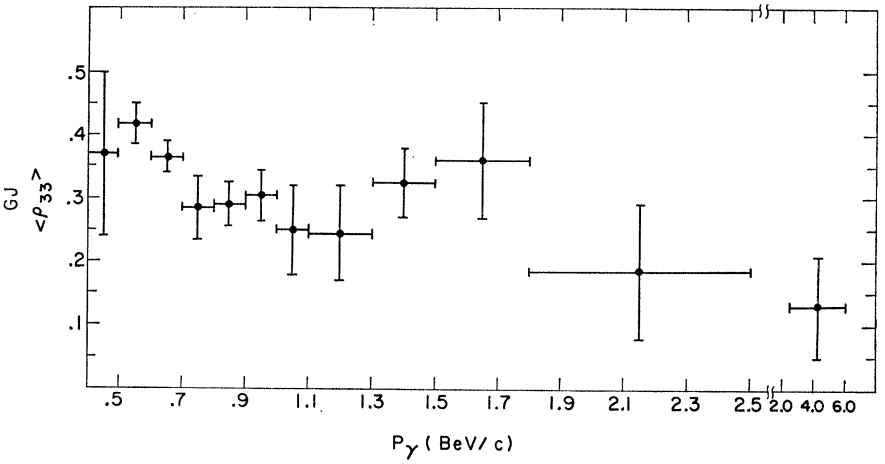

FIG. 8. Experimental spin-density matrix elements $\langle\rho_{33}^{GJ}\rangle$, describing the Gottfried–Jackson decay angular distribution for the Δ^{++} decay.

would not give rise to the other features discussed earlier, which are predicted by the resonance model.[21]

A further test of the production mechanisms responsible for reaction (3) is provided by the distribution of the Treiman-Yang angle ϕ, which is the angle between the $\Delta^{++}+\pi^-$ production plane and the decay plane of the $\Delta^{++}\to p+\pi^+$. The observed distributions are plotted in Fig. 9, in which we have combined the data at angles $\phi>90°$ with those for $\phi<90°$ by reflecting the distributions about $\phi=90°$. This improves the statistics of our comparison with the predictions, and is reasonable since the ϕ distributions (when averaged over the production and decay angles) are always expected to be of the form

$$W(\phi)=A+B\cos^2\phi. \tag{13}$$

Also shown in Fig. 9 are the predictions of the resonance model [see Eqs. (A4) and (A10)] with the same parameters as have been used in the previous comparisons. The corresponding density matrix element $\langle\mathrm{Re}(\rho_{3,-1})\rangle$, as a function of P_γ, is shown in Fig. 7.

Generally, the distributions are isotropic, as are the predictions. However, there seems to be a definite disagreement in the same low-energy region, in which we have noted also a discrepancy in the Adair angular distributions ($P_\gamma=0.4$–0.7 BeV/c; see Figs. 6, 7, and 9, and the discussion above). Again it is worth mentioning that the best fit obtained with the $\frac{3}{2}^-$ resonance shifted to 1460 MeV, which improves the Adair angular distribution as mentioned above, also improves the Treiman–Yang distribution (broken line in Fig. 7).

In summary, the observed decay angular correlations are in fair qualitative agreement with the resonance model, but a shift to a lower mass value for the $\frac{3}{2}^-$ resonance is required to account for the observed decay distributions at the lowest energies. The agreement for the production angular distribution obtained by using the 1512- and 1688-MeV isobars is generally improved by inclusion of a moderate amount of 1420-MeV isobar excitation, although the opposite is the case for the Adair and Treiman–Yang angular distributions. The fitting of our data does not require an appreciable amount of the 1924-MeV resonance. On the other hand, these data are in striking contradiction to the expectations of the conventional OPE model for the reaction $\gamma+p\to\Delta+\pi$.

E. Further Comments on the OPE Model

In the preceding discussions, we have commented in passing on the inadequacy of the conventional OPE model [Fig. 1(a)] for explaining the details of our observations. We present here some more detailed comparisons with the predictions of this model.[4,18]

Figure 10 is a comparison of the total cross section for Δ production as a function of the energy of the incident photon with the OPE predictions for small momentum transfers ($|t|\leq 10\ \mu^2$) and assuming maxi-

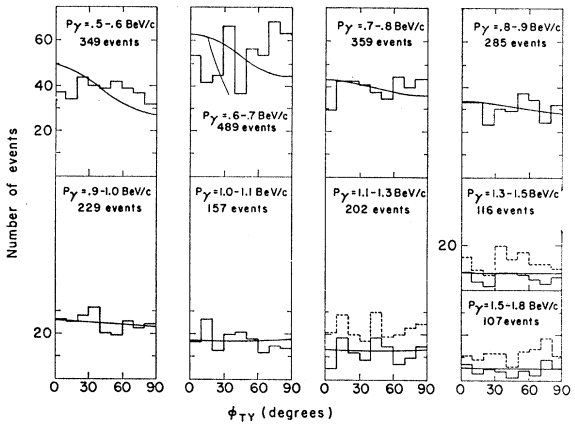

FIG. 9. The Treiman–Yang angular distributions for the Δ^{++} decay. The curves are calculated on the basis of the y_t's of row (4b) of Table III. For $P_\gamma>1.1$ BeV/c, the broken histograms represent the data before background subtraction.

[21] Furthermore, the total cross section for $\gamma+p\to\Delta+\pi$ is expected to increase (indeed, in a simple calculation, without form factors, it diverges) with increasing photon energy. In addition, the value of the coupling $g_{\gamma\pi\rho}$ required to account for the observed cross sections is excessively large; see Ref. 3.

mum S-wave absorption in the final state. Since OPE is expected to work best for small $|t|$, and since our cross sections are generally larger than the OPE predictions, this comparison is the most favorable one for the OPE hypothesis. [Our other assumptions as to the strengths of the couplings at the two vertices in Fig. 1(a) are the same as those of Drell.[4]]

Figure 11 shows our differential production cross section $d\sigma/dt$ for a number of photon energies, together with the OPE predictions derived on the same basis as for Fig. 10. (The data are, of course, the same as for Fig. 5, only the scales of the abscissa are different.) We note that the reasonable agreement, shown in Figs. 10 and 11, between our data and the OPE predictions for $E_\gamma \gtrsim 1$ BeV, may be somewhat misleading in view of normalization problems consistently encountered in OPE calculations.[22] The normalization we have used generally results in an overestimation of the cross sections for production of high-spin resonances.

The decay angular distributions of the Δ isobar, predicted by the OPE theory, have been mentioned earlier (Sec. II D). One expects, in this theory, a $1+3\cos^2\beta$ distribution over the entire energy range, namely $\langle \rho_{33}{}^{GJ} \rangle = 0$. The introduction of maximum absorption in the final state leads to a slow growth of the spin-density matrix element $\langle \rho_{33}{}^{GJ} \rangle$ from about 0.02 at our lowest energies to ~ 0.10 for $E_\gamma = 6.0$ BeV. It is clear from our observations, as shown in Fig. 8, that there is complete disagreement between our data and the OPE theory, for $E_\gamma < 1.8$ BeV.

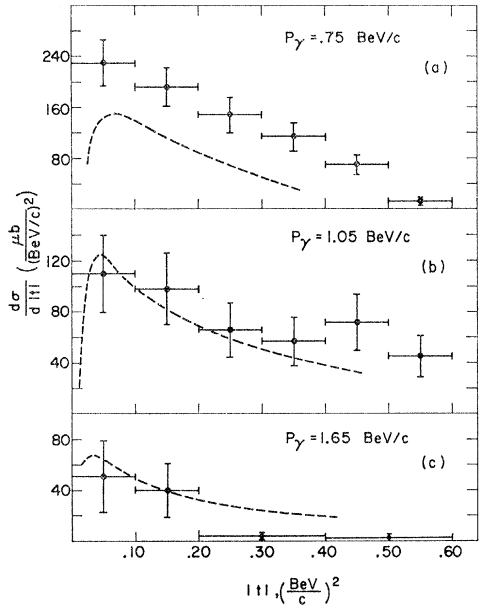

FIG. 11. Comparison of $d\sigma/d|t|$ for $\gamma+p \to \Delta^{++}+\pi^-$, at several photon energy intervals, with predictions of the conventional OPE theory, with maximum S-wave absorption in the final state: (a) $E_\gamma = 0.7$–0.8 BeV, (b) $E_\gamma = 1.0$–1.1 BeV, (c) $E_\gamma = 1.5$–1.8 BeV.

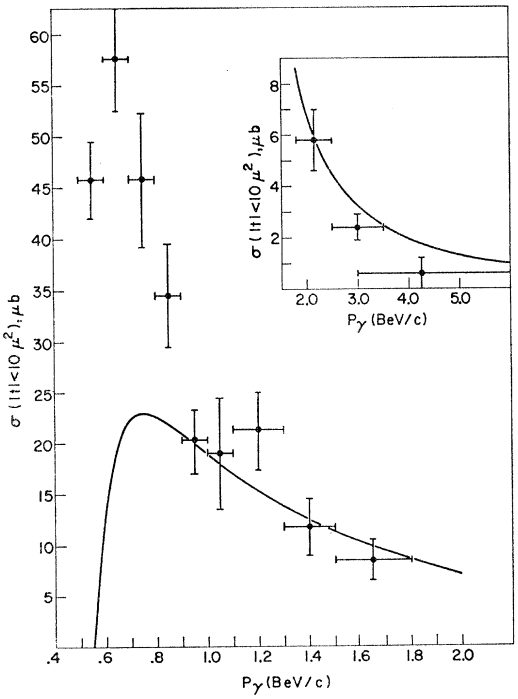

FIG. 10. Comparison of the cross section for $\gamma+p \to \Delta^{++}+\pi^-$ with predictions of the conventional OPE theory for invariant 4-momentum transfers to the Δ^{++} of $|t| < 10\ \mu^2$ and maximum ($\eta = 1$) S-wave absorption in the final state.

These comparisons confirm our previous comments as to the inadequacy of the conventional OPE model for explaining our observations. The ABBHHM collaboration has reached a similar conclusion.[5]

III. SUMMARY AND CONCLUSIONS

Observations have been described on double-pion production through the reaction $\gamma+p \to p+\pi^+ +\pi^-$ in the energy range 0.4–6.0 BeV. Below the ρ^0-meson production threshold, this reaction is dominated by the production of the Δ^{++} isobar. ρ^0-meson production having been discussed in detail in a previous communication,[3] we have confined ourselves in this paper to the reaction $\gamma+p \to \Delta+\pi$, which accounts for most of what remains of the $p\pi^+\pi^-$ events after subtraction of the ρ^0 channel. The data are very well described by a model in which the reaction proceeds through the photoexcitation of the known higher nucleon isobar—$N^{**}(1420)$, $N^{**}(1512)$, $N^{**}(1688)$, and possibly $N^{**}(1924)$.

This simple resonance model is successful in accounting for most of the observed features of the reaction $\gamma+p+ \to \Delta+\pi$ in the energy range $E_\gamma = 0.4$–1.8 BeV with a small number of *ad hoc* assumptions or adjustable parameters; the same relative resonance strengths which result in a best fit of the total-cross-section curve,

[22] J. D. Jackson, J. T. Donohue, K. Gottfried, R. Keyser, and B. E. Y. Svensson, Phys. Rev. **139**, B428 (1965); H. Hogaasen, J. Hogaasen, R. Keyser, and B. E. J. Svensson, Nuovo Cimento **42A**, 326 (1966).

account well for the production angular distributions, although not quite so well for the Δ decay angular correlations. As previously stated, the ABBHHM collaboration[5] has had some success in interpreting data very similar to ours with the model of Stichel and Scholz.[6] It is not clear how much their agreement could be improved by addition of resonant contributions, according to the diagram of [Fig. 1(b)], to the other terms in the Stichel–Scholz theory. On the other hand, it is most likely that, at the higher energies, our agreement would be improved by the addition of at least a moderate amount of OPE. The availability of more detailed and improved data should make it possible to determine the relative importance of these two complementary mechanisms.

ACKNOWLEDGMENTS

We are pleased to express our appreciation to the staff of the CEA for making available the facilities of the accelerator laboratory and the photon beam, to our scanning and computing groups for their efficient aid in the analysis of these data, to Dr. P. C. M. Yock for valuable discussions and aid in the theoretical aspects of this paper, and to S. Sen for extensive computations on the predictions of the resonance model.

APPENDIX: DERIVATION OF PRODUCTION AND DECAY ANGULAR DISTRIBUTIONS IN THE ISOBAR PHOTOEXCITATION MODEL

We consider the process

$$\gamma+p\rightarrow N_j^{**}\rightarrow\Delta+\pi^-,\quad \searrow\ p+\pi^+,$$

in which N_j^{**} represents any of the higher nucleon isobars which can decay into the Δ_{33} isobar plus a pion. The differential cross section for the reaction $a+b\rightarrow c+d$ in the c.m. system is given in the helicity representation by[23]

$$\frac{d\sigma}{d\Omega}=\frac{1}{2S_a+1}\frac{1}{2S_b+1}\sum_{[\lambda_i]}|\langle\lambda_c\lambda_d|T|\lambda_a\lambda_b\rangle|^2, \quad \text{(A1)}$$

with

$$\langle\lambda_c\lambda_d|T|\lambda_a\lambda_b\rangle=\frac{1}{2ik}\sum_J(2J+1)\langle JM\lambda_c\lambda_d|T^J|JM\lambda_a\lambda_b\rangle d_{\lambda\mu}{}^J(\theta_{\text{c.m.}}),$$

where S_a and S_b are the spins of the incident particles (for γ rays, $2S_\gamma+1=2$), λ_i is the helicity state of particle i, $d_{\lambda\mu}{}^J$ are the rotation matrices, $\lambda=\lambda_a-\lambda_b$, $\mu=\lambda_c-\lambda_d$, and k is the c.m. momentum in the initial channel. The sum over $[\lambda_i]$ indicates all possible sets of helicity states λ_a, λ_b, λ_c, λ_d.

For calculations in the isobar photoexcitation model it is convenient to transform the amplitudes from the $|JM\lambda_a\lambda_b\rangle$ representation into the $|JMLS\rangle$ representation. Thus we shall write[23]

$$\frac{1}{2ik}\langle JM\lambda_c\lambda_d|T^J|JM\lambda_a\lambda_b\rangle=\sum_{LSL'S'}C_{LSL'S'}{}^{\lambda\mu}\langle JML'S'|T^J|JMLS\rangle, \quad \text{(A2)}$$

where

$$C_{LSL'S'}{}^{\lambda\mu}=\left[\frac{(2L+1)(2L'+1)}{(2J+1)^2}\right]^{1/2}\langle J\lambda|L\tfrac{1}{2}\lambda_a-\lambda_b\rangle\times\langle J\mu|L'S'0\mu\rangle\langle S'\mu|S_cS_d\lambda_c-\lambda_d\rangle,$$

and the $\langle jm|j_1j_2m_1m_2\rangle$ are the usual Clebsch–Gordan coefficients. The term $\langle J\lambda|C\tfrac{1}{2}\lambda_a-\lambda_b\rangle$ represents the total-angular-momentum addition in the initial state; a γ ray with total angular momentum (multipolarity) L and helicity λ_a is combined with a proton of helicity λ_b to give the total J of the initial state with $J_z=\lambda$. L' is the final-state $\Delta+\pi$ orbital angular momentum.

So far our treatment is general and exact. In the isobar photoexcitation model we shall assume that the only nonvanishing amplitudes in expression (A2) are those $\langle JML'S'|T|JMLS\rangle$ which correspond to the intermediate isobars given in Table II of the text and having the quantum numbers as indicated in Table II. We shall further assume that the energy dependence of these amplitudes is given by a Breit–Wigner expression, Eq. (7) of the text. Note also that in using the form of Eq. (7) for the amplitudes, we explicitly assume that the $1/k$ term in Eq. (A2) is cancelled by a term $\sim k$ in the energy dependence of the partial widths, $\Gamma(N_j^*\rightarrow N+\gamma)$ [see also Ref. (13)].

We have altogether 16 helicity amplitudes in Eq. (A1), 8 with positive helicity (+1) for the γ ray, and 8 with negative (−1) helicity. The positive-helicity states are related to the negative-helicity states through parity conservation. It should be remembered that the positive-helicity amplitudes for electric multipoles contain an extra minus sign.[24] Each helicity amplitude contains at most four terms, given by Eq. (7), one for each of the isobars given in Table II. Note that only the lowest γ-ray multipoles and l_π values of Table II have been used. The higher terms have been neglected.

Using the above procedure we obtain the c.m. angular distribution for Δ production by incident unpolarized photons on an unpolarized target in the isobar photo-

[23] We follow here the notation of M. Jacob and G. C. Wick, Ann. Phys. (N. Y.) 7, 404 (1959).

[24] See J. M. Blatt and V. F. Weisskopf, *Theoretical Nuclear Physics* (John Wiley & Sons, Inc., New York, 1952), p. 808.

excitation model:

$$4\pi\,(d\sigma/d\Omega)=y_1^2|A_1|^2+y_2^2|A_2|^2+\tfrac{4}{5}y_3^2|A_3|^2(1+\tfrac{3}{4}\cos^2\theta)$$
$$+(11/24)y_4^2|A_4|^2[1+(285/22)\cos^2\theta-(360/11)\cos^4\theta+(525/22)\cos^6\theta]$$
$$+[y_1y_2\,\mathrm{Re}A_1A_2^*+3(\tfrac{3}{5})^{1/2}y_2y_3\,\mathrm{Re}A_2A_3^*]\cos\theta-\tfrac{3}{2}y_2y_4\,\mathrm{Re}A_2A_4^*\cos\theta(3-5\cos^2\theta)$$
$$-(\sqrt{\tfrac{3}{5}})y_1y_3\,\mathrm{Re}A_1A_3^*(1-3\cos^2\theta)+\tfrac{3}{8}y_1y_4\,\mathrm{Re}A_1A_4^*(1-10\cos^2\theta+(35/3)\cos^4\theta)$$
$$+\tfrac{1}{8}(\sqrt{\tfrac{3}{5}})y_3y_4\,\mathrm{Re}A_3A_4^*(1-58\cos^2\theta+(275/3)\cos^4\theta). \quad \text{(A3)}$$

The normalization is such that the total cross section is as given by Eq. (6), namely,

$$\sigma_T=y_1^2|A_1|^2+y_2^2|A_2|^2+y_3^2|A_3|^2+y_4^2|A_4|^2.$$

The decay angular distributions of the Δ_{33} resonance in its own rest frame are given, as usual,[4] in terms of the spin-space density matrix elements $\rho_{mm'}$:

$$W(\theta')=\tfrac{1}{4}(1+3\cos^2\theta')+\rho_{33}(1-3\cos^2\theta'),$$
$$W(\phi)=(1/2\pi)[1-(4/\sqrt{3})\,\mathrm{Re}\rho_{3,-1}\cos2\phi]. \quad \text{(A4)}$$

The density matrix is given by

$$\rho_{mm'}=\frac{1}{N}\sum_{\lambda_d\lambda_a\lambda_b}\langle m\lambda_d|T|\lambda_a\lambda_b\rangle\langle m'\lambda_d|T|\lambda_a\lambda_b\rangle^*. \quad \text{(A5)}$$

The unit trace condition of the density matrix must be satisfied, and thus

$$N=2(\rho_{33}+\rho_{11})=4d\sigma/d\Omega. \quad \text{(A6)}$$

In general, the density matrix is a function of the c.m. production angle. Thus, Eq. (A4) is also a function of the production angle. In this experiment, our data are insufficient for a detailed study of the production angle dependence of $\rho_{mm'}$. Therefore we wish to calculate the average value of $\rho_{mm'}$ over all production angles. These averages are given by

$$\langle\rho_{mm'}\rangle=\frac{1}{\sigma_T}\int\frac{d\sigma}{d\Omega}\rho_{mm'}d\Omega. \quad \text{(A7)}$$

Using Eqs. (A1)–(A7) we get the density matrix for the helicity angles (the angle between the Δ decay and the π^-, all in the Δ rest frame). The matrix element of interest here is ρ_{33}, and we get

$$\langle\rho_{33}{}^H\rangle=\frac{y_2^2|A_2|^2+\frac{4}{5}y_3^2|A_3|^2+(545/192)y_4^2|A_4|^2}{4(y_1^2|A_1|^2+y_2^2|A_2|^2+y_3^2|A_3|^2+y_4^2|A_4|^2)}. \quad \text{(A8)}$$

The density matrix with respect to any other axis of quantization is given by the usual rotation:

$$\rho=d^{3/2}(\psi)\rho^H d^{3/2}(-\psi), \quad \text{(A9)}$$

where ψ is the angle between the helicity axis and the new axis. For the Adair angular distribution (angle of the decay particle in the Δ rest frame with respect to the over-all c.m. z axis, i.e., γ-ρ c.m. axis) we get a simple expression, since we have here $\psi=\theta_{\text{c.m.}}$. The result is

$$\langle\rho_{33}{}^A\rangle=(1/4\sigma_T)[y_1^2|A_1|^2+\tfrac{3}{2}y_2^2|A_2|^2+\tfrac{3}{5}y_3^2|A_3|^2$$
$$+(33/28)y_4^2|A_4|^2-\tfrac{2}{3}(\sqrt{\tfrac{3}{5}})y_1y_3\,\mathrm{Re}(A_1^*A_3)],$$

and

$$\langle\mathrm{Re}\rho_{3,-1}{}^A\rangle=-(\sqrt{3}/4\sigma_T)[\tfrac{1}{3}y_1^2|A_1|^2+(1/15)y_3^2|A_3|^2$$
$$-(5/14)y_4|A_4|^2-(4/9)(\sqrt{\tfrac{3}{5}})y_1y_3\,\mathrm{Re}(A_1A_3^*)$$
$$+(17/36)(\sqrt{\tfrac{3}{5}})y_3y_4\,\mathrm{Re}(A_3A_4^*)$$
$$+\tfrac{1}{6}y_1y_4\,\mathrm{Re}(A_1A_4^*)]. \quad \text{(A10)}$$

From (A10) and (A4) we get the Adair and Treiman–Yang decay angular distributions, which are compared in the text with our experimental observations.